Strain-induced improper ferroelectricity in Ruddlesden-Popper perovskite halides

Yajun Zhang,[1,2] M. P. K. Sahoo,[1,3] Takahiro Shimada,[4] Takayuki Kitamura,[4] and Jie Wang[1,2,*]

[1]*Department of Engineering Mechanics, School of Aeronautics and Astronautics, Zhejiang University, Zheda Road 38, Hangzhou 310027, China*

[2]*Key Laboratory of Soft Machines and Smart Devices of Zhejiang Province, Zhejiang University, Zheda Road 38, Hangzhou 310027, China*

[3]*Department of Physics, RGUKT IIIT, Nuzvid Campus, Andhra Pradesh, India*

[4]*Department of Mechanical Engineering and Science, Kyoto University, Nishikyo-ku, Kyoto 615-8540, Japan*

(Received 6 June 2017; revised manuscript received 24 August 2017; published 19 October 2017)

Activating multiple symmetry modes and promoting a strong coupling between different modes by strain are indispensable to stabilize a polar ferroelectric (FE) phase from a nonpolar perovskite. Herein, through first-principles calculations, we propose an undiscovered and general avenue to engineering ferroelectricity in photovoltaic perovskites with a Ruddlesden-Popper (RP) structure. It is demonstrated that an experimentally accessible compressive strain can induce an in-plane polarization in RP perovskite halides thin films, resulting in an unusual paraelectric to FE phase transition. The detailed analysis on structure and energy reveals that the unusual FE phase transition in the perovskite halides stems from the strong coupling between strain and antiferrodistortive (AFD) mode. Further calculations show that the strain-AFD coupling-induced ferroelectricity is not only exhibited by perovskite halides but also observed in perovskite sulfides such as $Ba_3Zr_2S_7$. Moreover, it is found that the strained FE thin film possesses a suitable band gap of 1.6 eV for photovoltaic application. These findings not only unfold a general way to engineering nonpolar-to-polar transition, but also open an avenue to design optimal FE semiconductors for solar cell applications.

DOI: 10.1103/PhysRevB.96.144110

I. INTRODUCTION

ABX_3 (A = Cs, B = Sn, X = I, Br or Cl), a class of halide perovskites, has become a popular topic and attracted considerable interest due to their excellent photovoltaic properties [1]. Among these intriguing systems, iodides (X = I) and bromides (X = Br), which possess visible-region band gap and low effective mass, have garnered continuous attention over the last few years [2–4]. Moreover, it has been demonstrated in experiments that $CsSnI_3$ has a remarkably high mobility of hole at room temperature and could significantly enhance the absorption of visible light, especially on the red side of the spectrum [5]. All these features make $CsSnI_3$ an important candidate for solar cell applications. Recently, it was demonstrated that ferroelectricity plays an important role in photovoltaic materials [6–10]. Several mechanisms have been proposed to explain the enhancement of photovoltaic efficiency in ferroelectrics: (i) ferroelectrics lack the inversion symmetry, which provides an effective way to separate the carriers due to the bulk photovoltaic effect (BPVE) [11–15]; (ii) it is demonstrated experimentally and theoretically that potential steps could be produced at ferroelectric (FE) domain walls, which may help to separate the carriers within domain walls [16–18]; and (iii) depolarization field in FE film generated by incomplete screened polarization charges could enhance the separation of carriers and affect the photovoltaic output [19–22]. If ferroelectric polarization could be induced in perovskite halides, the inversion symmetry breaking promotes the desirable separation of photoexcited carriers and the incomplete screened polarization charge at domain walls and surfaces induces the depolarization field, which is useful for the enhancement of photovoltaic efficiency in these materials.

Perovskite-based Ruddlesden-Popper (RP) structure, characterized by stacking of the AX-terminated ABX_3 perovskite, has attracted great attention due to its fascinating physical and chemical properties [23–26]. The atomically thin geometry makes this class of two-dimensional layered materials display unique properties that parent materials do not possess. Especially, ferroelectricity has been theoretically demonstrated [27] and experimentally observed [28] at room temperature in the RP $A_3B_2O_7$ system, which holds great promise for enhancing the efficiency of photovoltaic applications. On the other hand, RP perovskites have drawn significant interest in photovoltaic devices, because it shows excellent performance compared to three-dimensional (3D) bulk materials in solar cells [26]. The insufficient long-term stability in 3D perovskites can be solved by "slicing" the 3D frameworks into well-defined RP structures [24]. The RP layered perovskite devices are demonstrated to be more stable over long-term operation against light soaking and humidity compared with 3D perovskite devices [26].

Given the great advantage of RP perovskites as photovoltaic materials and growing demand for engineering ferroelectricity in perovskite halides, it becomes significantly important to investigate the ferroelectricity in RP halides such as $Cs_3Sn_2I_7$. Moreover, strain engineering in perovskite oxides thin film has been intensively studied due to its scientific significance [29–31] and potential application in the magnetoelectric [32–35], photoelectric [36–39], and FE devices [40,41]. However, for strain engineering in promising RP perovskite halides, the interplay between strain, lattice distortion, and electronic properties has not been experimentally reported and remains uninvestigated theoretically, to the best of our knowledge.

In this work, we predict from first-principles calculations an unconventional coupling between strain and AFD mode in the perovskite halides of $Cs_3Sn_2I_7$ and $Cs_3Sn_2Br_7$ with RP structure, which can induce an unusual in-plane FE

*jw@zju.edu.cn

polarization under a compressive strain. In RP perovskite oxides, a FE $Cmc2_1$ phase is often the ground state. However, the perovskite halides $Cs_3Sn_2I_7$ and $Cs_3Sn_2Br_7$ exhibit a ground state of PE $P4_2/mnm$ phase, in which the intriguing PE-FE transitions can be achieved by compressive strain. Furthermore, the strained FE halides possess a much lower band gap than RP $A_3B_2S_7$, making them more suitable for absorbing a wide range of light spectrum. The present work suggests not only an unpredicted phase-transition behavior but also a useful RP photovoltaic candidate that facilitates both the light absorption and charge separation.

II. METHOD

We perform first-principles calculations based on the projector-augmented wave potentials [42,43] with Perdew-Burke-Ernzerhof revised for solids (PBEsol) functionals [44], which are implemented in the Vienna *ab initio* simulation package (VASP) [43,45]. To accurately determinate the band gap, the hybrid HSE06 functional [46] with an exchange screening parameter of 0.2 $Å^{-1}$ is used. The Brillouin zone is sampled using 6×6×4 and 6×6×2 for ABX_3 and $A_3B_2X_7$ compounds, respectively [47]. Careful test calculations show that a relatively high plane-wave cutoff energy of 500 eV can get well-converged results. The geometry structure is fully optimized until the Hellmann-Feynman forces on the atoms are less than 0.01 eV/Å. The ISOTROPY programs are utilized for the lattice mode and group theoretical analysis [48]. The spontaneous polarization P is obtained by the Berry-phase approach [49].

III. RESULTS

A. Paraelectric phase of strain-free $Cs_3Sn_2I_7$ and $Cs_3Sn_2Br_7$

To verify the accuracy of the present methods, the electronic and structural properties of orthorhombic $CsSnI_3$ and $CsSnBr_3$, i.e., the primitive materials for the RP $A_3B_2X_7$ compounds, are calculated first. It is experimentally observed that $CsSnI_3$ exhibited a cubic phase ($Pm\bar{3}m$) above 426 K and an orthorhombic phase ($Pnma$) below 352 K [50]. For $CsSnBr_3$, both cubic and tetragonal phases are observed in experiments [51,52]. Nevertheless, recent phonon-dispersion analysis has demonstrated that the $Pnma$ phase is dynamically stable rather than cubic or tetragonal phases [53]. Thus, in the following we will focus on the $Pnma$ phase of $CsSnI_3$ and $CsSnBr_3$. The band gaps of $CsSnI_3$ and $CsSnBr_3$ are predicted to be 1.3 and 1.45 eV, respectively, from the HSE06 functional, which are in good agreement with the experiments [54]. The fully relaxed $CsSnI_3$ has the lattice constants of $a = 8.76$ Å, $b = 8.41$ Å, and $c = 12.26$ Å, which have the errors of 0.9, 2.7, and 1.0%, respectively, compared to the experimental results [50]. The structure is also relaxed with the PBE functional; the corresponding errors are 2.8, 0.8, and 1.1%, respectively. Note that the PBEsol functional overestimates the value of b, while the PBE functional overestimates the value of a. Since phase transitions and critical strain are sensitive to the lattice constant, the PBE functional is also used for the prediction of phase transitions in the next section.

Next, the FE distortion of the RP structures of $CsSnI_3$ and $CsSnBr_3$ is studied. Previous work studied the electronic properties of $Cs_3Sn_2I_7$, but structural and FE properties have not yet been investigated [55]. To determine the corresponding RP structures with minimum energies, we perform fully structural optimization by imposing individual and/or coupled distortion modes to distortion-free $I4/mmm$ phase. To make sure of the reliability of the present work, we have calculated the phonon curve of cubic $CsSnI_3$ and impose similar unstable modes into the $I4/mmm$ phase. These modes include (i) AFD modes, namely in-phase rotation along the [001] axis (irreducible representations (irrep) X_2^+), out-of-phase rotation along the [001] axis (irreps X_1^-), and out-of-phase rotation around the [110] or [100] axis (irreps X_3^-), (ii) in-plane polarization along the [110] direction (irreps Γ_5^-), and (iii) antipolar mode (irreps M_5^+). Similar modes have been considered in previous work to analyze the stability of RP $I4/mmm$ perovskite oxides [56]. It should be noted that computing different distortion models in a cubic CsSnI3 system and remapping them onto the layered RP system in the present work is an approximate method. Although the approximation can qualitatively reflect the phonon instability in the RP structure [57], the QUANTUM ESPRESSO density-functional theory should be employed for more accurate calculations [58]. After the change of supercell size and atomic position relaxation, the energies of $P4_2/mnm$, $Pbcn$, $Ccca$, and $Cmc2_1$ phases are obtained for different strains as shown in Fig. S1 of Supplemental Material [59]. In contrast to widely investigated RP perovskite oxides like $Ca_3Ti_2O_7$ and $Ca_3Mn_2O_7$, the ground states (GSs) of $Cs_3Sn_2I_7$ and $Cs_3Sn_2Br_7$ without strain are found to be nonpolar $P4_2/mnm$ phase. Although $A_3B_2X_7$ halides structure has not been reported experimentally, $Ba_3Zr_2S_7$ containing a large X atom has been synthesized in experiments and exhibits the PE $P4_2/mnm$ phase [60]. Thus, it is expected that $A_3B_2X_7$ halides structure has the similar properties and could be synthesized in experiments. The distortion mode of the GS and the energy difference between PE $P4_2/mnm$ and FE $Cmc2_1$ phases are listed in Table I in the absence of strain. The energies of the FE $Cmc2_1$ phases are 44 and 35 meV higher than those of PE GSs for $Cs_3Sn_2I_7$ and $Cs_3Sn_2Br_7$, respectively Unlike bulk $CsSnI_3$ and $CsSnBr_3$, in which octahedral rotation and tilting modes coexist, the state of $P4_2/mnm$ phase is characterized only by octahedral tilting about the [100] direction as shown in Table I. Group theory analysis shows that the Γ_1^+ mode, which is induced by Cs and I or Br displacements along the c axis, also exists in the GS. Since two adjacent Cs-I or Cs-Br layers displace along opposite directions with the same amplitude, the system keeps the PE state. Thus, the conclusion can be drawn that only out-of-phase tilting exists in RP $Cs_3Sn_2I_7$ and $Cs_2Sn_3Br_7$, and no FE distortion is predicted in the absence of strain.

TABLE I. The amplitude of mode in the $P4_2/mnm$ phase from ISOTROPY results and the energy difference between the $P4_2/mnm$ ground state and the ferroelectric $Cmc2_1$ phase for $Cs_3Sn_2I_7$ and $Cs_3Sn_2Br_7$ in the absence of strain.

	Γ_1^+	Γ_5^-	X_1^-	X_2^+	X_3^-	ΔE
$Cs_3Sn_2I_7$ (PE)	2.41	0	0	0	2.35	−44 meV
$Cs_3Sn_2Br_7$ (PE)	2.27	0	0	0	2.01	−35 meV

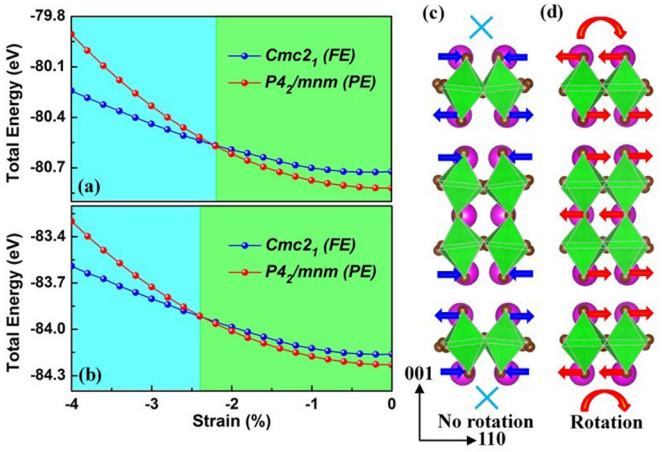

FIG. 1. Phase diagrams of (a) $Cs_3Sn_2I_7$ and (b) $Cs_3Sn_2Br_7$ as a function of compressive strain; (c) $P4_2/mnm$ and (d) $Cmc2_1$ structures of $Cs_3Sn_2I_7$ without strain and with 2.4% compressive strain, respectively. The arrows denote the atomic displacements of A-site atoms.

B. Unusual paraelectric to ferroelectric phase transition

Now let us turn our attention to the effect of strain on the structural and FE properties of $Cs_3Sn_2I_7$ and $Cs_3Sn_2Br_7$. The biaxial strain is imposed by varying lattice constant along both the [100] and [010] directions. The biaxial in-plane compressive strain is defined as $\varepsilon_{11} = \varepsilon_{22} = (l - l_0)/l_0$, where l_0 and l are the in-plane equilibrium lattice length of unstrained $P4_2/mnm$ phase ($a = b = l_0$) and strained states ($a = b = l$), respectively. For the strained states, the sizes of calculated supercell are fixed in the [100] and [010] directions, respectively, while it can change in the [001] direction during the relaxation. With these assumptions, stresses in the [100] and [010] directions are homogeneous, which can be expressed as $\sigma_{11} = \sigma_{22} = \varepsilon_{11}c_{11} + \varepsilon_{22}c_{12} + \varepsilon_{33}c_{13}$, where σ_{ij} is the stresses and c_{ij} is the elastic constants. To investigate the possible phase transitions, Figs. 1(a) and 1(b) illustrate the variations of energy of FE and PE phases for $Cs_3Sn_2I_7$ and $Cs_3Sn_2Br_7$ as a function of strain. The energies of different phases of RP $Sr_3Zr_2O_7$ have also been calculated under different strains as a comparison as shown in Fig. S1(a) [59], in which the FE-PE phase transition takes place. This FE-PE phase transition is consistent with previous result [56], indicating that the present calculation methods are reliable. For halide perovskites, however, it is found that there is a PE-FE phase transition under compressive strains. The energy of the PE $P4_2/mnm$ phase is lower than that of the FE $Cmc2_1$ phase when strain is less than -2.4% (-2.6) for $Cs_3Sn_2I_7$ ($Cs_3Sn_2Br_7$), whereas the FE phase has a lower energy when strain is beyond -2.4% (-2.6%). As shown in Figs. 1(c) and 1(d), the experimentally accessible compressive strain transfers the GS of RP $Cs_3Sn_2I_7$ from the nonpolar $P4_2/mnm$ phase to the polar $Cmc2_1$ phase. To check the reliability of the calculations, the results from PBE functional are also shown in Fig. S2 of Supplemental Material [59]. The same phase transitions are found in the materials although the critical strain is a little bit different, which further confirms the unusual PE-FE phase transition under compressive strains. In order to check whether ferroelectricity can be retained at room temperature, we estimate the Curie temperature according to Ref. [61]; the energy loss between PE $I4/mmm$ phase and FE $Cmc2_1$ phase (4% compressive strain) is 0.206 eV/f.u. (0.493 eV/f.u. in Ref. [61]), which corresponds to a Curie temperature of about 459 K (1100 K in Ref. [61]).

To give insight into the underlying physical mechanism of the unusual PE-FE phase transitions, the detailed analysis on lattice distortion is performed. For RP perovskite oxides, as demonstrated in Ref. [56], as compressive strain increases, the in-phase rotation vanishes and out-of-phase rotation appears at the phase boundary. As a result, the $Cmc2_1$ (FE) to $Pbcn$ (PE) phase transition takes place. However, the evolution of the distortion mode for RP perovskite halides is totally different from that of RP perovskite oxides. Figures 2(a) and 2(b) show the strain dependence of the rotation and tilting modes in

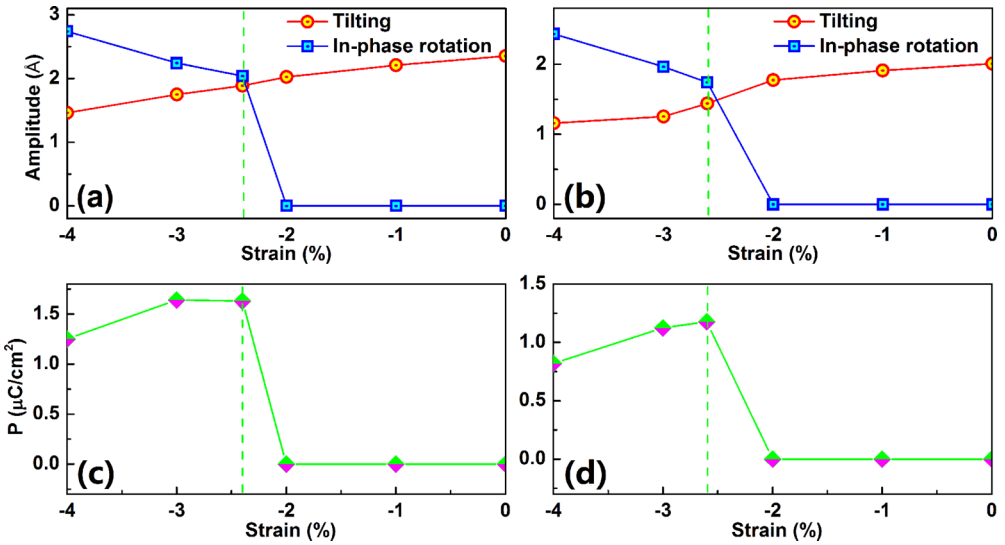

FIG. 2. The dependence of the rotation and tilting modes for (a) $Cs_3Sn_2I_7$ and (b) $Cs_3Sn_2Br_7$ as a function of strain. Ferroelectric polarization of (c) $Cs_3Sn_2I_7$ and (d) $Cs_3Sn_2Br_7$ from Berry-phase method.

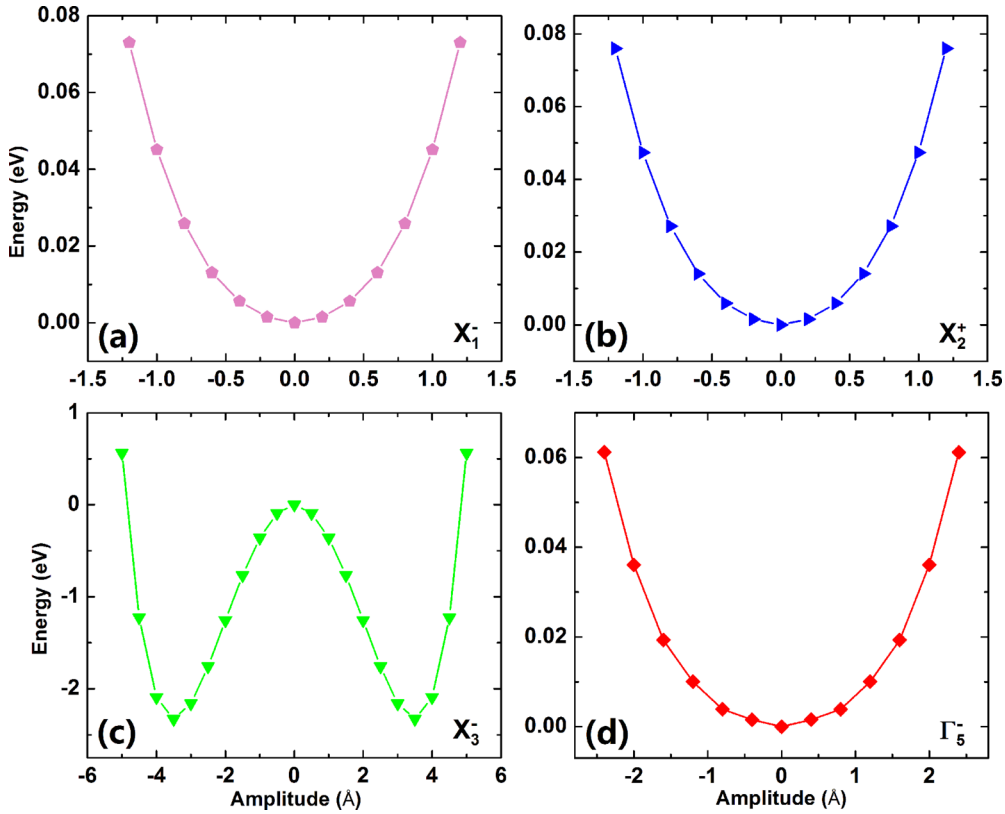

FIG. 3. The energy curves of four symmetry modes (X_1^-, X_2^+, X_3^-, and Γ_5^-) for $Cs_3Sn_2I_7$ without strain. The energy of high-symmetry $I4/mmm$ phase is treated as the reference.

$Cs_3Sn_2I_7$ and $Cs_3Sn_2Br_7$, respectively. There is no rotation in the PE region. The detailed atomic structure can be found in Fig. 1(c). In-phase rotation suddenly appears at the phase boundary and gradually increases under compressive strains. This may be the main reason for the different transition behavior of RP $Cs_3Sn_2X_7$ from that of $Sr_3Zr_2O_7$ subjected to a compressive strain. Recently, it is found that polarization could be induced by a trilinear improper coupling among the octahedral rotation, tilting, and polarization in the form of PQ_1Q_2 in Landau free-energy expansion [28,62]. For $Cs_3Sn_2I_7$ and $Cs_3Sn_2Br_7$ under compressive strains as shown in Fig. 1(d), strain-induced rotation mode together with existing tilting mode are responsible for the hybrid improper ferroelectricity (HIF).

A deeper understanding of the phase transitions can be obtained by examining the contribution of individual mode to the total energy of the system. We take the distortion-free $I4/mmm$ phase as the reference; Fig. 3 shows the energy curves of four symmetry modes (X_3^-, X_2^+, X_1^-, and Γ_5^-) for strain-free $Cs_3Sn_2I_7$. It is found that there is a double-well energy profile only for the X_3^- mode. This indicates that in-phase octahedral rotation is completely suppressed and HIF is unfavorable for strain-free $Cs_3Sn_2I_7$. The same phenomenon is found in $Cs_3Sn_2Br_7$. Figures 4(a) and 4(b) show the energy curves of X_2^+ and X_3^- mode as a function of distortion amplitude in $Cs_3Sn_2I_7$ with 2.4% compressive strain. The tilting energies associated with the X_3^- keep a double-well potential, indicating that the tilting mode always exists in the GS. In addition, the depth of the double-well decreases compared with that of the strain-free state. This is consistent with the mode variation of X_3^- displayed in Fig. 2(a), which shows that compressive strain suppresses the tilting mode. For in-phase rotation X_2^+ mode, when 2.4% compressive strain is imposed, an intriguing double-well potential emerges and the symmetry of the system is further broken toward a new phase where the octahedral rotation is more favored. To investigate the validity of ferroelectricity in the strained state, we plot the energy change with respect to the amplitude of Γ_5^- for $Cs_3Sn_2I_7$ under 2.4% compressive strain in Fig. 4(c). The energy curve exhibits a single-well potential, indicating the in-plane polar mode is stable. When octahedral rotation and tilting modes are imposed, the minimum energy of Γ_5^- as shown in Fig. 4(d) shifts to a nonzero value, indicating the emergence of hybrid improper ferroelectricity. From the above analysis, we can conclude that the coupling of strain and AFD leads to the appearance of in-phase rotation at the phase boundary, where the unusual PE-FE phase transition takes place.

C. Ferroelectric semiconductor for photovoltaic applications

It is well known that perovskite halides are important candidates for solar cell application due to their visible-region band gaps and high mobility of hole [50]. For the improvement of perovskite solar cell efficiency, the ability to precisely tailor the electronic structure and get a suitable band gap is crucial for practical application. We further investigate the band gap of $Cs_3Sn_2I_7$ compounds. Figure 5 shows the range of the band gap in the PE and FE region, respectively. It is found that the

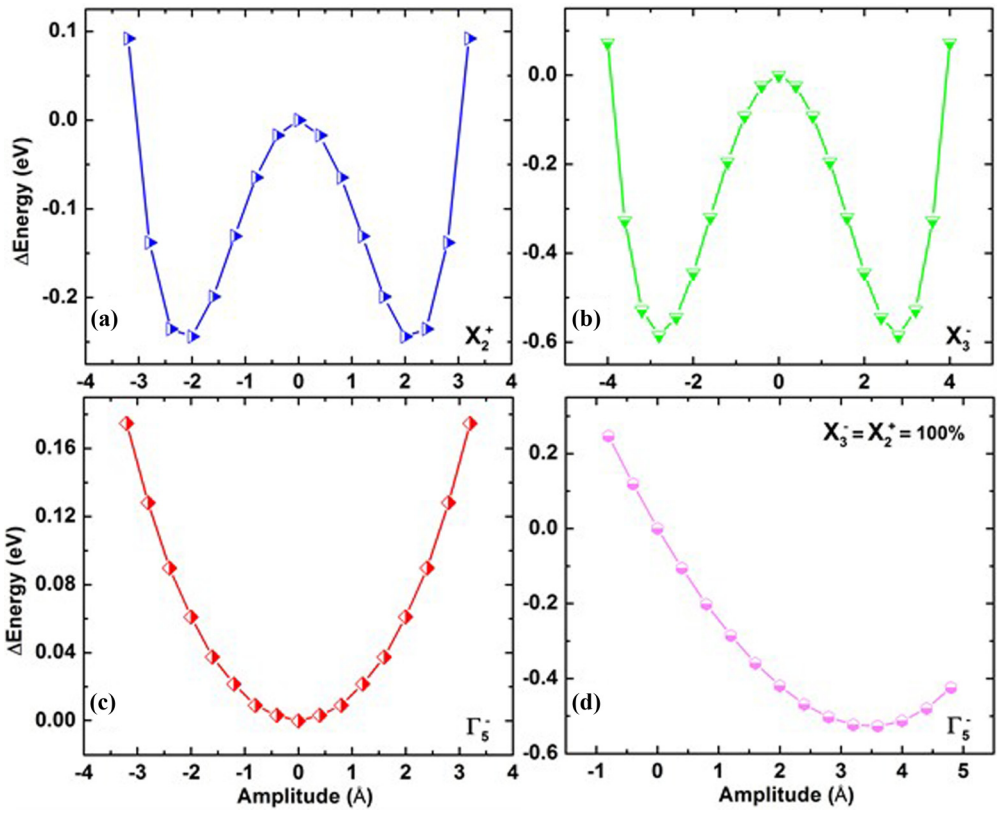

FIG. 4. Evolution of energy difference with respect to the energy with zero-mode amplitude for (a) in-phase rotation mode, (b) tilting mode, (c) purely polar mode, and (d) polar mode with initial rotation and tilting modes that have the same amplitude as the ground state of $Cs_3Sn_2I_7$ under 2.4% compressive strain. The high-symmetry $I4/mmm$ phase is treated as the reference structure.

band gap of PE $Cs_3Sn_2I_7$ ranges from 1.15 to 1.20 eV between 0 and -2% strain. For FE $Cs_3Sn_2I_7$, the band gap is a little bit increased, ranging from 1.57 to 1.76 eV between -2.4 and -4% strain. Compared to the lowest band gap of 2.7 eV of perovskite oxides $BiFeO_3$ [18] and RP perovskite sulfides $Ca_3Zr_2S_7$ (2.18 eV) [63], the relatively lower band gap of perovskites halides could increase the absorption of sunlight in a wide range of the visible-light spectrum. It should be noted that the band gap jumps by about 0.4 eV at the phase boundary, which provides an effective way to control the photovoltaic property. To get insight into the change of band gap during the phase transition, we have carefully checked the density of states of the phases at the phase-transition boundary and the effect of different distortions on the valence-band maximum (VBM) and conduction-band minimum (CBM) of the system. Similar to previous works on the $CsSnI_3$ system [39], we found that strain-induced polar mode has negligible effect on the electronic structure. In contrast, the in-phase rotation induced by compressive strain has a notable effect on the VBM and CBM states. The position of CBM increases slightly and the energy level of CBM decreases significantly. Thus, the band gap of FE phase increases due to the appearance of rotation. Moreover, ferroelectricity has been recently demonstrated to play an important role in the separation of photoexcited carriers in perovskite solar cell devices. Thus, it is meaningful to explore the modulation of FE polarization by epitaxial compressive strain. Figures 2(c) and 2(d) show the amplitudes of the in-plane polarization under different strains for $Cs_3Sn_2I_7$ and $Cs_3Sn_2Br_7$, respectively. The polar phase is used as the ground state under different strains, and the high-symmetry $I4/mmm$ phase is taken as reference. We use the same method as Ref. [64] for the calculation of polarization, in

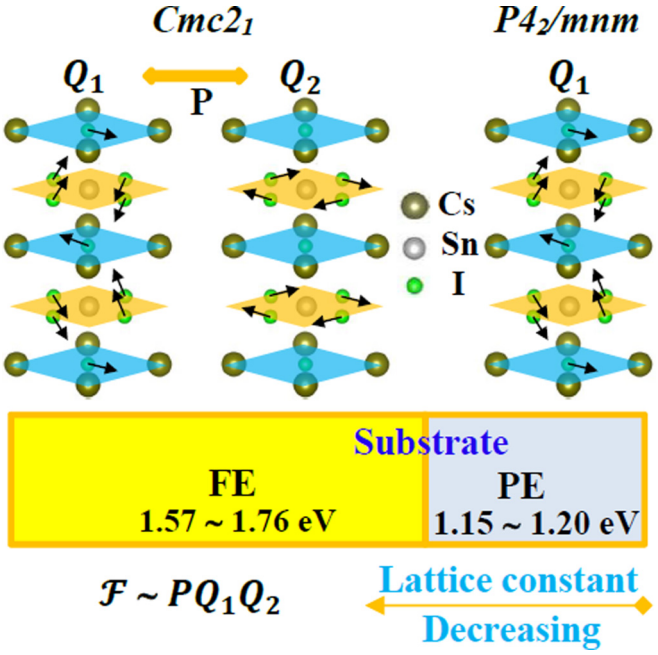

FIG. 5. Mechanism of the PE-FE transition and the band gap in the PE and FE region for $Cs_3Sn_2I_7$. Q_1 denotes the tilting mode and Q_2 represents the in-phase rotation mode.

which a series of structures with different percentages of polar mode and polarization indetermination quantum defined as eR/V are considered. Two materials show the same trend for polarization: under the moderate strains from 0 to −2%, the polarization is zero. When the compressive strain is beyond 2.4% (2.6% for $Cs_3Sn_2Br_7$), notable polarization about 1.6 (1.2) $\mu C/cm^2$ appears in $Cs_3Sn_2I_7$ ($Cs_3Sn_2Br_7$) thin film. The polarization amplitude slightly decreases with the increase of compressive strain due to the decreased tilting mode. Even though the amplitude of polarization is much smaller than traditional ferroelectrics such as $BiFeO_3$ and $PbTiO_3$, the small polarization is useful for photovoltaic applications due to the following reasons: (i) the origin of BPVE in FE materials is the noncentrosymmetric nature but not the amplitude of polarization [11–15]. Although $Cs_3Sn_2I_7$ contains small polarization, it is enough to break the symmetry and induce BPVE to enhance the photocurrent; and (ii) the relationship between shift current response and polarization is quite complex. A larger polarization does not always mean a larger shift current response. For example, $PbTiO_3$ exhibits a similar shift current response with $BaTiO_3$ despite the polarization amplitude of $PbTiO_3$ being two times larger than that of $BaTiO_3$ [9]. In addition, it is found that $MAPbI_3$ possesses a comparable shift current magnitude with that of $BiFeO_3$, despite having a very small polarization (5 $\mu C/cm^2$) [65]. Thus, the present work suggests a potential avenue to design the low-band-gap FE semiconductors of $Cs_3Sn_2I_7$ and $Cs_3Sn_2Br_7$, which may maximize the absorption of wide-range spectrum and enhance their performance as photovoltaic materials.

The "engineering" of ferroelectricity in strained thin film has long been a promising paradigm for creating FE materials. With the development of first-principles calculations, FE materials have been proposed. The mechanism of the PE-FE transitions in ABO_3 perovskite oxides is usually the direct coupling between polarization and strain, no matter in incipient ferroelectrics [66–70], misfit superlattices [71], or large strained perovskites [35,72]. In the present work, the polarization in RP perovskite halides is contributed not by the direct coupling with strain but by the strain-AFD coupling. Although strain-AFD coupling has been discussed in $(PbTiO_3)_1/(SrTiO_3)_1$ superlattices [62,73], its coupling mechanism is quite different from the present case. The polarization in $(PbTiO_3)_1/(SrTiO_3)_1$ superlattices stems from both the proper ferroelectricity of $PbTiO_3$ and the trilinear coupling between polarization and rotation modes. Furthermore, the direct coupling between strain and polarization makes a significant contribution to the total strain-controlled polarization of the superlattices due to the strong FE-strain coupling in individual $SrTiO_3$ and $PbTiO_3$ layers. In the present RP perovskite halides, there is no direct coupling between strain and polarization. The polarization is purely contributed by the strain-AFD coupling; the mechanism of this coupling is clearly shown in Fig. 5. When $Cs_3Sn_2I_7$ grows on a substrate with a small lattice constant, the compressive strain will promote the appearance of in-phase rotation; in-plane polarization is automatically induced due to the trilinear coupling. Therefore, we propose a strain-AFD coupling induced nonpolar-to-polar transition in perovskite system. In addition, we further demonstrate that strain-AFD coupling-induced ferroelectricity exhibits not only in perovskite halides but also in the photovoltaic sulfides material such as $Ba_3Zr_2S_7$ (as shown in Fig. S3 of Supplemental Material [59]), making it a general way to induce ferroelectricity in the $P4_2/mnm$ PE phase. Due to the recently dramatic progress on the synthesis of RP $A_3B_2X_7$ ferroelectrics [28,61] and high-quality epitaxial grown technology [29], we hope RP perovskite halides and sulfides with small compressive epitaxial strain will be synthesized in the future.

IV. SUMMARY

In conclusion, the effect of strain on the structural, energetic, and electronic properties of Ruddlesden-Popper perovskite halides of $Cs_3Sn_2I_7$ and $Cs_3Sn_2Br_7$ has been investigated by first-principles calculations. It is found that an experimentally accessible compressive strain can induce an in-plane polarization in the perovskite halide thin films, resulting in an unusual paraelectric to ferroelectric phase transition. Furthermore, unlike the direct coupling between strain and polarization in most perovskite oxides, the strong coupling between strain and antiferrodistortive mode is found in the perovskite halides, which is responsible for the unusual ferroelectric phase transition. This could be a general way to engineering ferroelectricity in $P4_2/mnm$ paraelectric phase such as $Ba_3Zr_2S_7$. It is also found that the strained ferroelectric halides possess a semiconductor property with a suitable band gap for absorbing sunlight in a wide range of the visible-light spectrum. Thus, the present work not only uncovers an unusual ferroelectric phase transition but also suggests an avenue to design ferroelectric photovoltaic compounds from perovskite halides.

ACKNOWLEDGMENTS

We thank Dr. Eric Bousquet for the helpful discussion. The work was financially supported by the National Natural Science Foundation of China (Grants No. 11472242, No. 11672264, and No. 11621062), Zhejiang Provincial Natural Science Foundation (Grant No. LZ17A020001), and the Fundamental Research Funds for the Central Universities (Grant No. 2017FZA4030). The calculations in this work were conducted at the National Supercomputing Center of Guangzhou, China.

[1] W.-J. Yin, J.-H. Yang, J. Kang, Y. Yan, and S.-H. Wei, J. Mater. Chem. A **3**, 8926 (2015).

[2] M. H. Kumar, S. Dharani, W. L. Leong, P. P. Boix, R. R. Prabhakar, T. Baikie, C. Shi, H. Ding, R. Ramesh, M. Asta *et al.*, Adv. Mater. **26**, 7122 (2014).

[3] P. Xu, S. Chen, H.-J. Xiang, X.-G. Gong, and S.-H. Wei, Chem. Mater. **26**, 6068 (2014).

[4] K. P. Marshall, M. Walker, R. I. Walton, and R. A. Hatton, Nat. Energy **1**, 16178 (2016).

[5] I. Chung, B. Lee, J. Q. He, R. P. H. Chang, and M. G. Kanatzidis, Nature (London) **485**, 486 (2012).

[6] I. Grinberg, D. V. West, M. Torres, G. Gou, D. M. Stein, L. Wu, G. Chen, E. M. Gallo, A. R. Akbashev, P. K. Davies, J. E. Spanier, and A. M. Rappe, Nature (London) **503**, 509 (2013).

[7] T. Choi, S. Lee, Y. Choi, V. Kiryukhin, and S.-W. Cheong, Science **324**, 63 (2009).

[8] Y. Zhang, M. P. K. Sahoo, and J. Wang, J. Phys. Chem. Chem. Phys. **19**, 7032 (2017).

[9] S. M. Young and A. M. Rappe, Phys. Rev. Lett. **109**, 116601 (2012).

[10] Z. Fan, K. Sun, and J. Wang, J. Mater. Chem. A **3**, 18809 (2015).

[11] A. A. Grekov, M. A. Malitskaya, V. D. Spitsina, and V. M. Fridkin, Sov. Phys. Crystallogr. **15**, 423 (1970).

[12] V. M. Fridkin, A. A. Grekov, P. V. Ionova, A. I. Rodin, E. A. Savchenko, and K. A. Mikhailina, Ferroelectrics **8**, 433 (1974).

[13] B. S. I. Sturman and V. M. Fridkin, *Photovoltaic and Photorefractive Effects in Noncentrosymmetric Materials* (Gordon and Breach, Philadelphia, 1992).

[14] A. M. Glass, D. von der Linde, and T. J. Negran, Appl. Phys. Lett. **25**, 233 (1974).

[15] S. M. Young, F. Zheng, and A. M. Rappe, Phys. Rev. Lett. **109**, 236601 (2012)

[16] S. Y. Yang, J. Seidel, S. J. Byrnes, P. Schafer, C.-H. Yang, M. D. Rossel, P. Yu, Y.-H. Chu, J. F. Scott, J. W. Ager, III, L. W. Martin, and R. Ramesh, Nat. Nanotechnol. **5**, 143 (2010).

[17] J. Seidel, L. W. Martin, Q. He, Q. Zhan, Y.-H. Chu, A. Rother, M. E. Hawkridge, P. Maksymovych, P. Yu, M. Gajek, N. Balke, S. V. Kalinin, S. Gemming, F. Wang, G. Catalan, J. F. Scott, N. A. Spaldin, J. Orenstein, and R. Ramesh, Nat. Mater. **8**, 229 (2009).

[18] J. Seidel, D. Fu, S.-Y. Yang, E. Alarcon-Llado, J. Wu, R. Ramesh, and J. W. Ager, Phys. Rev. Lett. **107**, 126805 (2011).

[19] A. G. Chynoweth, Phys. Rev. **102**, 705 (1956).

[20] W. Ji, K. Yao, and Y. C. Liang, Adv. Mater. **22**, 1763 (2010).

[21] L. Pintilie, I. Vrejoiu, G. Le Rhun, and M. Alexe, J. Appl. Phys. **101**, 064109 (2007).

[22] M. Qin, K. Yao, and Y. C. Liang, Appl. Phys. Lett. **95**, 022912 (2009).

[23] M. S. Senn, A. Bombardi, C. A. Murray, C. Vecchini, A. Scherillo, X. Luo, and S. W. Cheong, Phys. Rev. Lett. **114**, 035701 (2015).

[24] C. C. Stoumpos, D. H. Cao, D. J. Clark, J. Young, J. M. Rondinelli, J. I. Jang, J. T. Hupp, and M. G. Kanatzidis, Chem. Mater. **28**, 2852 (2016).

[25] A. T. Mulder, N. A. Benedek, J. M. Rondinelli, and C. J. Fennie, Adv. Funct. Mater. **23**, 4810 (2013).

[26] H. Tsai, W. Nie, J.-C. Blancon, C. C. Stoumpos, R. Asadpour, B. Harutyunyan, A. J. Neukirch, R. Verduzco, J. J. Crochet, S. Tretiak, L. Pedesseau, J. Even, M. A. Alam, G. Gupta, J. Lou, P. M. Ajayan, M. J. Bedzyk, M. G. Kanatzidis, and A. D. Mohite, Nature (London) **536**, 312 (2016).

[27] N. A. Benedek and C. J. Fennie, Phys. Rev. Lett. **106**, 107204 (2011).

[28] Y. S. Oh, X. Luo, F.-T. Huang, Y. Wang, and S.-W. Cheong, Nat. Mater. **14**, 407 (2015).

[29] D. G. Schlom, L. Q. Chen, C. B. Eom, K. M. Rabe, S. K. Streiffer, and J. M. Triscone, Annu. Rev. Mater. Res. **37**, 589 (2007).

[30] C. Ederer and N. A. Spaldin, Phys. Rev. Lett. **95**, 257601 (2005).

[31] M. Dawber, K. M. Rabe, and J. F. Scott, Rev. Mod. Phys. **77**, 1083 (2005).

[32] S. Bhattacharjee, E. Bousquet, and Ph. Ghosez, Phys. Rev. Lett. **102**, 117602 (2009).

[33] J. H. Lee and K. M. Rabe, Phys. Rev. Lett. **104**, 207204 (2010).

[34] T. Günter, E. Bousquet, A. David, P. Boullay, P. Ghosez, W. Prellier, and M. Fiebig, Phys. Rev. B **85**, 214120 (2012).

[35] H. J. Zhao, Y. Yang, W. Ren, A.-J. Mao, X. M. Chen, and L. Bellaiche, J. Phys.: Condens. Matter **26**, 472201 (2014).

[36] J. Varignon, N. C. Bristowe, and P. Ghosez, Phys. Rev. Lett. **116**, 057602 (2016).

[37] W. Zhang, M. M. Yang, X. Liang, H. W. Zheng, Y. Wang, W. X. Gao, G. L. Yuan, W. F. Zhang, X. G. Li, H. S. Luo, and R. K. Zheng, Nano Energy **18**, 315 (2015).

[38] C. H. Chiu, W. I. Liang, C. W. Huang, J. Y. Chen, Y. Y. Liu, J. Y. Li, C. L. Hsin, Y. H. Chu, and W.-W. Wu, Nano Energy **17**, 72 (2015).

[39] C. Grote and R. F. Berger, J. Phys. Chem. C **119**, 22832 (2015).

[40] H. H. Wu, J. M. Zhu, and T.Y. Zhang, Nano Energy **16**, 419 (2015).

[41] H. W. Jang, A. Kumar, S. Denev, M. D. Biegalski, P. Maksymovych, C. W. Bark, C. T. Nelson, C. M. Folkman, S. H. Baek, N. Balke, C. M. Brooks, D. A. Tenne, D. G. Schlom, L. Q. Chen, X. Q. Pan, S. V. Kalinin, V. Gopalan, and C. B. Eom, Phys. Rev. Lett. **104**, 197601 (2010).

[42] G. Kresse and D. Joubert, Phys. Rev. B **59**, 1758 (1999).

[43] P. E. Blöchl, Phys. Rev. B **50**, 17953 (1994).

[44] J. P. Perdew, A. Ruzsinszky, G. I. Csonka, O. A. Vydrov, G. E. Scuseria, L. A. Constantin, X. Zhou, and K. Burke, Phys. Rev. Lett. **100**, 136406 (2008).

[45] G. Kresse and J. Hafner, Phys. Rev. B **47**, 558 (1993).

[46] J. Heyd, G. E. Scuseria, and M. Ernzerhof, J. Chem. Phys. **124**, 219906 (2006).

[47] H. J. Monkhorst and J. D. Pack, Phys. Rev. B **13**, 5188 (1976).

[48] H. T. Stokes, D. M. Hatch, and B. J. Campbell (2007), ISOTROPY, http://stokes.byu.edu/isotropy.html.

[49] R. D. King-Smith and D. Vanderbilt, Phys. Rev. B **47**, 1651 (1993).

[50] I. Chung, J.-H. Song, J. Im, J. Androulakis, C. D. Malliakas, H. Li, A. J. Freeman, J. T. Kenney, and M. G. Kanatzidis, J. Am. Chem. Soc. **134**, 8579 (2012).

[51] M. Mori and H. Saito, J. Phys. C: Solid State Phys. **19**, 2391 (1986).

[52] J. Barrett, S. R. A. Bird, J. D. Donaldson, and J. Silver, J. Chem. Soc. A **1971**, 3105 (1971).

[53] L. Y. Huang and W. R. L. Lambrecht, Phys. Rev. B **90**, 195201 (2014).

[54] C. C. Stoumpos, C. D. Malliakas, and M. G. Kanatzidis, Inorg. Chem. **52**, 9019 (2013).

[55] C. Grote, B. Ehrlich, and R. F. Berger, Phys. Rev. B **90**, 205202 (2014).

[56] X. Z. Lu and J. M. Rondinelli, Nat. Mater. **15**, 951 (2016).

[57] T. Birol, N. A. Benedek, and C. J. Fennie, Phys. Rev. Lett. **107**, 257602 (2011).

[58] L. Louis and S. M. Nakhmanson, Phys. Rev. B **91**, 134103 (2015).

[59] See Supplemental Material at http://link.aps.org/supplemental/10.1103/PhysRevB.96.144110 for the phase diagrams of $Sr_3Zr_2O_7$, $Cs_3Sn_2I_7$, and $Cs_3Sn_2Br_7$ as a function of compressive strain from different functionals.

[60] Y. C. Hung, J. C. Fettinger, and B. W. Eichhorn, Acta Cryst. **53**, 827 (1997).
[61] X. Q. Liu, J. W. Wu, X. X. Shi, H. J. Zhao, H. Y. Zhou, R. H. Qiu, W. Q. Zhang, and X. M. Chen, Appl. Phys. Lett. **106**, 202903 (2015).
[62] E. Bousquet, M. Dawber, N. Stucki, C. Lichtensteiger, P. Hermet, S. Gariglio, J.-M. Triscone, and P. Ghosez, Nature **452**, 732 (2008).
[63] H. Wang, G. Gou, and J. Li, Nano Energy **22**, 507 (2016).
[64] J. B. Neaton, C. Ederer, U. V. Waghmare, N. A. Spaldin, and K. M. Rabe, Phys. Rev. B **71**, 014113 (2005).
[65] F. Zheng, H. Takenaka, F. Wang, N. Z. Koocher, and A. M. Rappe, J. Phys. Chem. Lett. **6**, 31 (2015)
[66] J. H. Haeni *et al.*, Nature (London) **430**, 758 (2004).
[67] O. Dieguez, K. M. Rabe, and D. Vanderbilt, Phys. Rev. B **72**, 144101 (2005).
[68] C.-J. Eklund, C. J. Fennie, and K. M. Rabe, Phys. Rev. B **79**, 220101 (2009).
[69] A. Antons, J. B. Neaton, K. M. Rabe, and D. H. Vanderbilt, Phys. Rev. B **71**, 024102 (2005).
[70] Y. Zhang, M. Liu, J. Wang, T. Shimada, and T. Kitamura, J. Appl. Phys. **115**, 224107 (2014).
[71] Y. Zhang, M. P. K. Sahoo, T. Shimada *et al.*, J. Phys.: Condens. Matter **27**, 385901 (2015).
[72] Y. Yang, W. Ren, M. Stengel, X. H. Yan, and L. Bellaiche, Phys. Rev. Lett. **109**, 057602 (2012).
[73] P. Aguado-Puente, P. Garcıa-Fernandez, and J. Junquera, Phys. Rev. Lett. **107**, 217601 (2011).